Direct Electromagnetic Coupling for Non-Invasive Measurements of Stability in Simulated Fracture Healing

Kevin M. Labus,[1] Conor Sutherland,[1] Branislav M. Notaros,[2] Milan M. Ilić,[3] George Chaus,[4] David Keiser,[5] Christian M. Puttlitz[1]

[1]Orthopaedic Bioengineering Research Laboratory, Department of Mechanical Engineering and School of Biomedical Engineering, Colorado State University, 1374 Campus Delivery, Fort Collins, ColoradoColorado 80523-137, [2]Department of Electrical and Computer Engineering, Colorado State University, Fort Collins, ColoradoColorado, [3]School of Electrical Engineering, University of Belgrade, Belgrade, Serbia, [4]Orthopaedic Trauma Surgery, Front Range Orthopaedics and Spine, Longmont, ColoradoColorado, [5]Department of Orthopaedic Surgery and Musculoskeletal Medicine, Christchurch School of Medicine, University of Otago, Christchurch Central, New Zealand

Received 7 August 2018; accepted 12 February 2019
Published online in Wiley Online Library (wileyonlinelibrary.com). DOI 10.1002/jor.24275

ABSTRACT: Diagnostic monitoring and prediction of bone fracture healing is critical for the detection of delayed union or non-union and provides the requisite information as to whether therapeutic intervention or timely revision are warranted. A promising approach to monitor fracture healing is to measure the mechanical load-sharing between the healing callus and the implanted hardware used for internal fixation. The objectives of this study were to evaluate a non-invasive measurement system in which an antenna electromagnetically couples with the implanted hardware to sense deflections of the hardware due to an applied load and to investigate the efficacy of the system to detect changes in mechanical load-sharing in an ex vivo fracture healing model. The measurement system was applied to ovine metatarsal bones treated with osteotomies, resulting in four different levels of bone stability which simulated various degrees of fracture healing. Computational finite element simulations supplemented these ex vivo experiments to compare the osteotomy model of fracture healing to a more clinically applicable callus stiffening model of healing. In the ex vivo experiments, the electromagnetic coupling system detected significant differences between the four simulated degrees of healing with good repeatability. Computational simulations indicated that the experimental model of fracture healing provided a good surrogate for studying healing during the early time period as the callus stiffness is increasing as well as when diagnostic monitoring of the healing process is most critical. Based upon the data reported herein, the direct electromagnetic coupling method holds strong potential for clinical assessments and predictions of fracture healing. © 2019 Orthopaedic Research Society. Published by Wiley Periodicals, Inc. J Orthop Res 37:1164–1171, 2019.

Keywords: fracture healing; diagnostic monitoring; electromagnetic coupling; load sensing

Orthopaedic extremity injuries present a large medical and financial burden to both the United States and worldwide communities. Approximately 7.9 million bone fractures are reported per annum in the United States, and about 10% of these fractures do not heal properly.[1] For injuries that involve a significant disturbance to the vascular supply, the rates of delayed union or non-union have been reported to be as high as 46%.[2] The most common complication is bony non-union, a chronic condition associated with pain and disability. It has been estimated that these deleterious effects and resultant costs can be reduced by at least 50% if complications associated with the non-union can be avoided or addressed during the early time period.[3]

Currently, clinicians usually monitor healing visually, using radiographs, and may examine the mechanical condition of the union via manually bending the bone at the fracture.[4,5] Unfortunately, the course of delayed or non-union fracture healing is not easily diagnosed in the early time period when standard radiographic information of the fracture site is not capable of discriminating the healing pathway due to the relative paucity of mineralized tissue.[6] Therefore, new technologies that provide diagnostic information as to the course of bone healing within the first four post-operative weeks may provide a significant impact on clinical orthopaedic practice and treatment of problematic fractures.

Complicated long bone fractures are usually treated with internal fixation devices, most commonly with screws and plates or intramedullary nails. It has been shown in clinical practice and via animal models that healing is critically related to the degree of fracture stability and implant load-sharing in the early time period.[2,7,8] Animal studies using wired strain gages have demonstrated that the healing callus and bone assume an increasing proportion of the load as fracture healing proceeds, reducing the burden on the implanted hardware.[9] If the healing is on course toward delayed union or non-union, this gradual transfer of the loading burden is altered or non-existent; i.e., the healing tissue cannot assume its normal share of the load because it does not have the structural or material capacity to do so.

To date, many of the technologies that seek to exploit this bone-implant load sharing phenomena have been considered too large in dimension or involve implantation of an associated power supply. Previous investigations have been successful in determining forces in the hip,[10–12] spine,[13–15] and shoulder.[16] However, due to the relatively large size of the sensors and associated hardware (signal conditioning, modulation, etc.), most of the aforementioned telemetry systems have been implanted inside of joint replacement components or bulky internal fixators.[17] The

Conflict of interest: None.

Correspondence to: Christian M. Puttlitz (T: (970) 491-0956; F: (970) 491-3872; E-mail: christian.puttlitz@colostate.edu)

result is that these devices have produced data that has developed our temporal understanding of bone-implant loading,[18] but, to date, have not been advantageous for large-scale implementation as a diagnostic and/or prognostic tool.

In order to overcome these aforementioned shortcomings, our group has developed a telemetry system that utilizes a biocompatible, micro-electro-mechanical system (bioMEMS) strain sensor, coupled with an external antenna.[19,20] The sensor is attached to the internal hardware device used to fix the fracture, and as the hardware is mechanically loaded, the sensor is deformed, changing the resonance of the coupled external antenna. We have used this system to report the temporal in vivo load-sharing of a fixation plate in a large animal model and conclusively shown that these data can be used to predict the fracture's healing cascade.[21] For fractures treated with external fixation, it has been proposed to utilize the implanted pins themselves as antennas to monitor fracture healing.[22] Whereas this approach detects changes in the electromagnetic properties of the tissue in the fracture space throughout healing, our group's approach uses external antennas to detect changes in the mechanical stability of the fracture.

Recent advancements have demonstrated the ability for an external antenna to directly couple with the fixation hardware already used ("direct electromagnetic coupling," DEC), eliminating the need for an implantable sensor to measure hardware deformations.[23] Whereas the bioMEMs sensor method uses deformation of the sensor circuit itself to detect changes in the resonant frequency, the DEC technique detects changes in distance between the hardware and the external antenna as the hardware is deformed (i.e., bending) under an applied load. Deflections of the hardware shift the resonant frequency of the antenna through electromagnetic near field effects. The theoretical foundations of this measurement technique have been recently demonstrated.[23] However, the fidelity of the DEC technique as it relates to monitoring fracture healing has not been previously examined. Accordingly, the objective of the current study was to investigate the efficacy of the DEC method for measuring changes in fracture stability associated with healing using both cadaveric experimental and computational methods.

METHODS

Direct Electromagnetic Coupling System

This investigation involved a series of physical experiment and associated simulations that were intended to determine the efficacy of the DEC method for predicting bone fracture healing. The DEC system consisted of a vector network analyzer (model: TTR503A, Tektronix, Beaverton, OR) used to create an excitation in a radio frequency antenna and measure the response of the $|S_{11}|$ parameter, defined as the ratio in dB of power reflected by the antenna to the power supplied to generate the initial signal. A target object in the vicinity couples with the antenna and alters the electromagnetic near field, thus shifting the Apparent Resonant Frequency (ARF) as determined from the measured $|S_{11}|$ parameter.[23] The ARF was defined as the frequency at which the $|S_{11}|$ sweep reaches a local minima in the response magnitude (dB). Therefore, the ARF represents the frequency at which the antenna is most efficiently radiating energy. The antenna used in the current investigation was optimized in a prior study and consisted of two parallel coaxial cables, each helically coiled in three loops.[23] This antenna exhibited a coupled ARF ranging from 395 to 440 MHz.

Modeled Fracture Healing Experiments

A series of cadaver experiments involved applying the DEC system to a large animal fracture fixation scenario. Our group has extensive in vitro and in vivo experience with this model, and it is well characterized for investigating fracture fixation and healing applications.[21,24–26]

A six-hole locking plate (P04028, Synthes, West Chester, PA) was instrumented with a wired strain gage rosette (MMF313001, Micro Measurements, Raleigh, NC) and fastened to metatarsal bones ($n = 7$) harvested from adult sheep hind limbs (sacrificed for unrelated studies). Because the tissue in the vicinity of the plate can affect the signal received by the antenna, no soft tissue was removed from the metatarsals, and the incision in the cutaneous tissue was closed via suturing after placement of the fracture plate. Each plated metatarsus was tested in compression under four variants which mechanically simulated different phases of fracture healing: Intact, 1-Cortical Osteotomy (1CO), 1.5-Cortical Osteotomy (1.5CO), and 2-Cortical Osteotomy (2CO). Specimens were first tested in a healthy, intact case to simulate a fully healed scenario. A saw blade was then used to create an osteotomy through one cortical surface by approaching from the contralateral cortical surface in order to simulate a relatively later stage of healing and higher stability (1CO). For the next treatment, the same saw blade osteotomy was further advanced partially through the cortical surface adjacent to the plate in order to simulate an earlier stage of healing (1.5CO), and hence, less stability. Finally, a full osteotomy was performed through both cortical surfaces simulating a complete fracture (i.e., immediately post-operative) in which the plate bears the entire load on the construct (2CO). Radiographs were used to guide and confirm the extent of each osteotomy defect (Fig. 1b).

The proximal and distal bones adjacent to the metatarsals on either end (tibia and phalanges, respectively) were fixed, and the construct was mounted on a servo-hydraulic testing machine (Bionix, MTS, Eden Prairie, MN; Fig. 1a). The antenna was attached to the construct using elastic straps. The bone-plate constructs were mechanically loaded in compression at a quasi-static rate from 0 to 500 N for five cycles. Similar loads were applied in a previous ovine in vivo model with no adverse effects on osseous healing.[21] Forces and moments were measured using a six degree-of-freedom load cell (MC3A-1 K, AMTI, Waterton, MA) while simultaneously measuring principal strain from the wired strain gage and ARF from the antenna. Because the signal from the antenna is sensitive to the antenna's placement, it was desirable to quantify the intra-subject repeatability of the wireless measurement system. Therefore, for each treatment of each specimen, the test was conducted with five repeti-

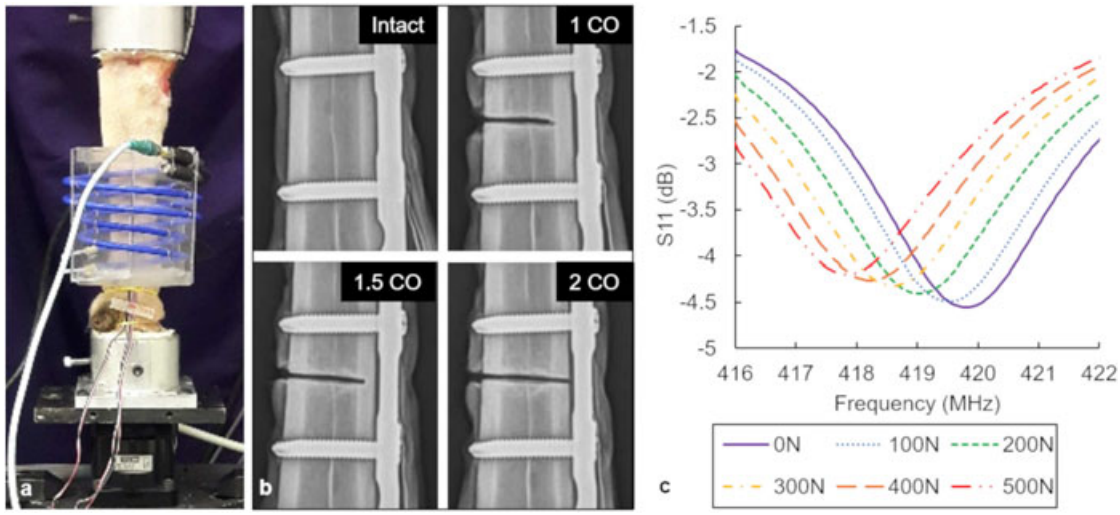

Figure 1. (a) Setup of the fracture fixation experiment with the antenna affixed to a metatarsal in the compressive testing frame. (b) Radiographs demonstrating the four osteotomy variants: Intact, 1 cortical osteotomy (1CO), 1.5 cortical osteotomy (1.5CO), and 2 cortical osteotomy (2CO). (c) $|S_{11}|$ sweep at multiple loads of an example specimen with a 2CO treatment.

tions. Between each repetition, the antenna was removed from the plate-bone construct and subsequently reattached.

It was of particular interest to determine the effects of the four treatments on the signal for each specimen individually in addition to analyzing the average response in order to account for the inherent inter-population variability that is encountered in both animal specimens and human patient populations. Therefore, the ARF/load, strain/load, and ARF/strain slopes were compared between the four treatments for each specimen individually, based on the five repetitions of each test. Statistical analyses were performed via two-way ANOVA with Student-Newman-Keuls post-hoc tests, with statistical significance set at $p < 0.05$.

Finite Element Simulations

A finite element simulation of the bone-plate experiment described above was developed. The finite element model was adapted from a validated ovine hind limb model previously published by our group.[24] The original model was recreated from computed tomography (CT) image data using AMIRA visualization software (version 5.0, VSG, Burlington, MA). The plate geometry was developed in SolidWorks to match dimensions of the plates used in the aforementioned experiments. The six locking screws were modelled as perfect cylinders, and tie constraints were used to rigidly couple the screws with the plate and bone. The distal aspect of the metatarsus was kinematically constrained (i.e., encastre boundary condition), and a 500N axial load was applied to the geometric center of the proximal surface of the metatarsus (Fig. 2a). Transversely isotropic material properties were assigned to the bone,[27–31] and linear elastic stainless steel properties ($E = 193$ GPa, $\nu = 0.29$) were assigned to the plate and screws. In order to closely simulate the experimental study, the finite element model was used to predict the principal strain in the plate under four different levels of construct stability by assigning a negligible elastic modulus ($E = 100$ Pa) to cortical bone sections within the projected fracture gap region (replicating the intact, 1CO, 1.5CO, and 2CO cases). Principal strain was predicted from a group of 34 surface nodes on the outer face of the plate in order to match the footprint of the strain gage in the experimental testing.

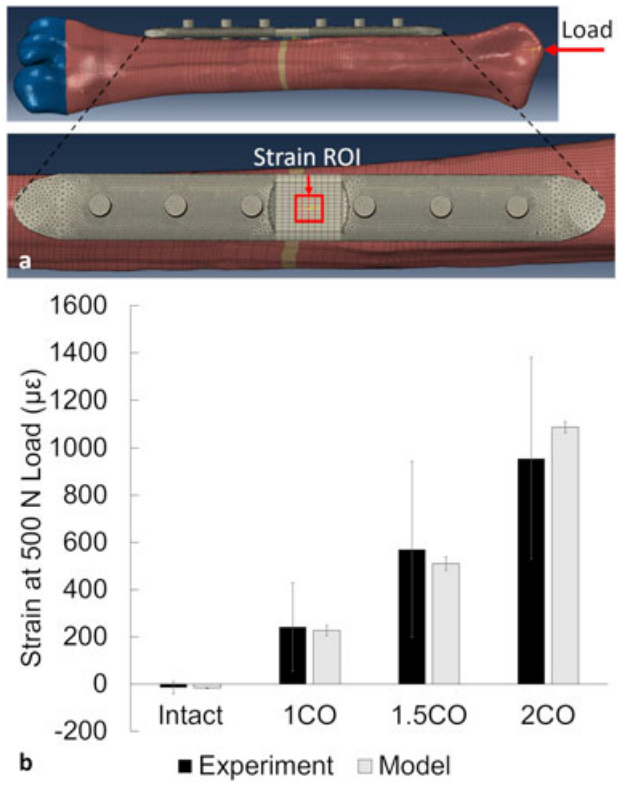

Figure 2. (a) Mechanical finite element model of the sheep metatarsal with attached fracture fixation plate, highlighting the region of interest (ROI, red square) that was designated for obtaining strain predictions (corresponding to the strain gage footprint in the physical experiments). The axial load application on the proximal head of the metatarsal and kinematic constraints on the distal metatarsal (blue elements) are shown. (b) Plate principal strains (mean and standard deviation) are plotted for the experimental data and the finite element model predictions. The finite element model standard deviation was obtained from the predictive variance within the 34 nodes in the ROI.

The relative deflection of the plate was predicted, defined as the displacement of a node on the center of the plate relative to two nodes at the contact points of the antenna frame, located 45 mm above and below the center of the plate.

While the aforementioned experimental and computational studies investigated discreet levels of bone-plate construct stability via specific removal of bone tissue elements, fracture healing is a gradual and continuous process wherein the callus temporally evolves with coincident increases in stiffness. Therefore, a parametric finite element study of callus elastic modulus was performed wherein the elements representing the fracture gap were increased from 1 kPa to 1 GPa. The callus was assigned isotropic properties to simulate the spectrum of disorganized soft tissue to woven bone composition during the fracture healing cascade. Both hardware strain and relative deflection were predicted and calculated from the same nodes as delineated above.

RESULTS

As evidenced by the profiles of the frequency sweeps of the $|S_{11}|$ parameter, the antenna measurement was able to detect a shift in the ARF due to the applied load (Fig. 1c). The ARF shift, applied load, and principal strain on the plate (as measured by the wired strain gage) were all compared. The ARF data exhibited a strong linear relationship with the applied load (mean $r^2 = 0.99$, Fig. 3a). Additionally, the intact case exhibited very small ARF shifts, and the magnitude of the shift increased progressively for each osteotomy treatment. Linear regression mean slopes from the ARF versus applied load curves increased accordingly with each progressively destabilizing treatment (Fig. 4a), and these slopes were significantly different between all treatments ($p < 0.04$).

Given the inherent differences in anatomy and plate fixation within the specimen population, each specimen was analyzed individually by determining the relative change in ARF versus load slope between treatments. The ARF-applied load slopes were significantly different ($p < 0.02$) between treatments for each specimen tested, with the exceptions being: (1) specimen #4 comparing intact and 1CO variants ($p = 0.11$); (2) specimen #6 comparing intact and 1CO ($p = 0.11$); and (3) specimen #6 comparing 1CO and 1.5CO ($p = 0.06$) (Fig. 5a). The average coefficient of variance of the five test repetitions per treatment was 8.5%.

The data obtained from the wired strain gage on the fixation plate also exhibited a linear relationship between the principal strain and the applied load (mean $r^2 = 0.98$, Fig. 3b). In each specimen, the deformation was very small (less than 50 με) for the intact treatment, and increased for each subsequently imposed osteotomy (1CO, 1.5CO, and 2CO). Similarly, the mean strain magnitude at 500 N load increased progressively for each osteotomy treatment ($p < 0.03$ between all treatments), indicating that the osteotomy treatments progressively destabilized the construct and increased the load share on the plate (Fig. 2b). When the specimens were analyzed individually, the slopes of the strain versus applied load curves were significantly different ($p < 0.01$) between all treatments for each specimen tested (Fig. 5b).

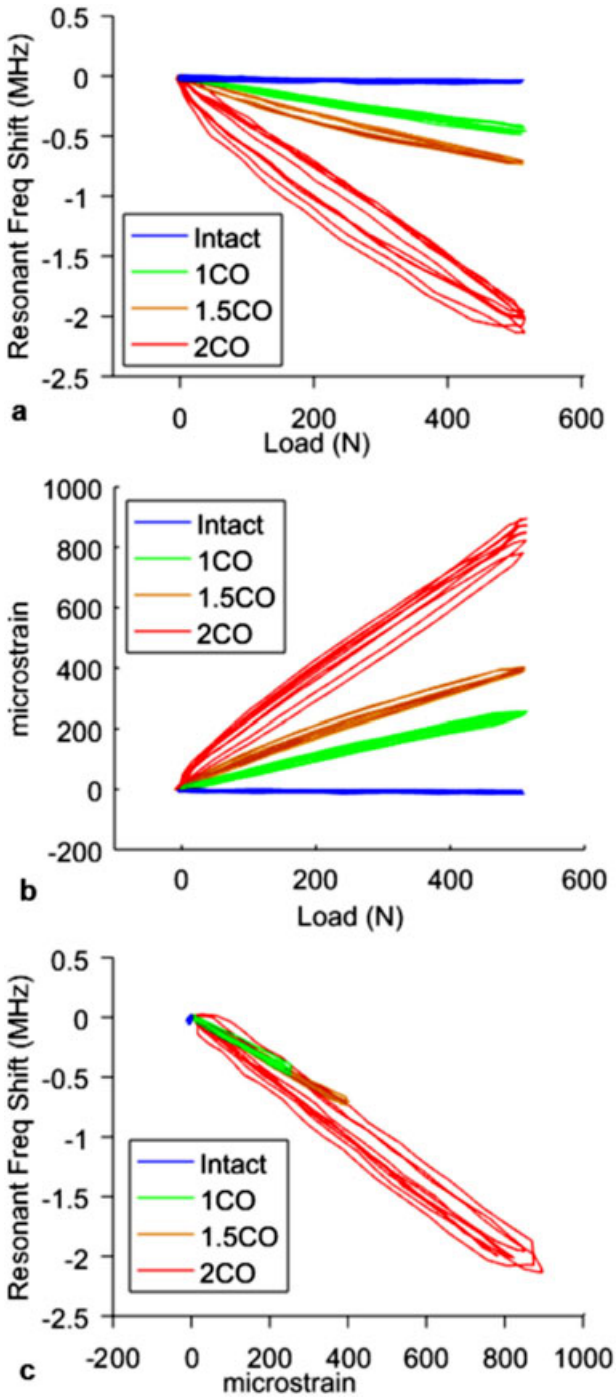

Figure 3. Measured data from an example specimen illustrating the last cycle (loading and unloading) of all 5 test repetitions for each condition. The plots demonstrate (a) ARF shift versus load, (b) strain versus load, and (c) ARF shift versus strain. These data demonstrate the highly linear relationships between these parameters and relative consistency of the data between testing repetitions.

In order to determine if the ARF shifts were proportional to changes in plate strain while also accounting for specimen-specific variables, the ARF shift and the change in strain (between 0 and 500 N)

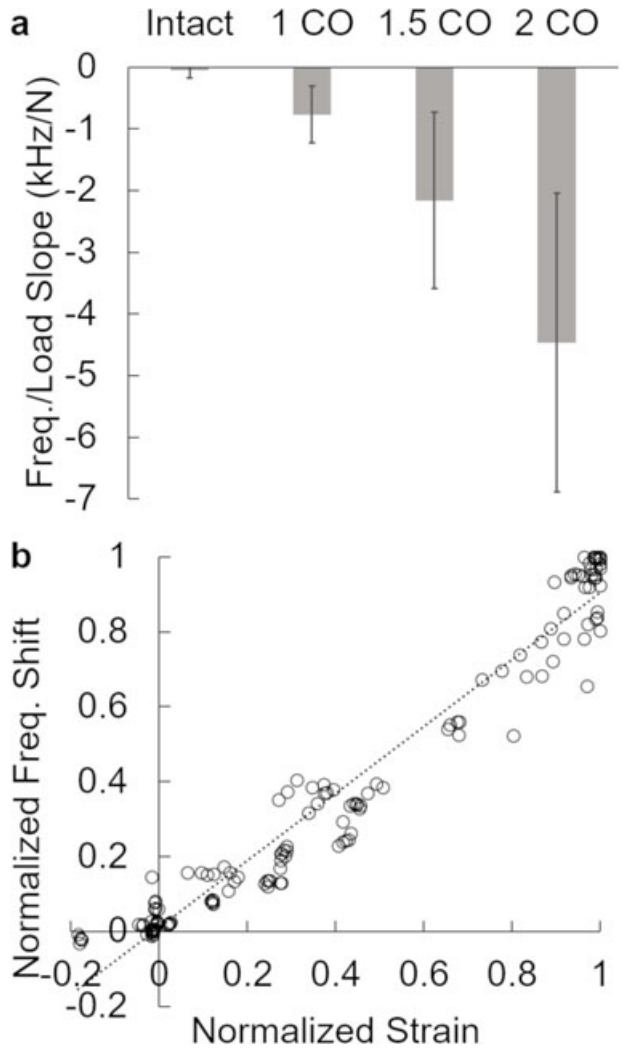

Figure 4. (a) Compiled linear regression slope data from the ARF versus load curves from all tested specimens (mean and standard deviation). Significant differences existed for all comparison of means between treatment groups ($p < 0.04$). (b) Normalized ARF shift versus normalized strain plotted for all test repetitions. A linear regression of the data showed a strong correlation ($r^2 = 0.95$), indicating that ARF shift was representative of plate strain.

were normalized to the maximum measured value for each particular specimen. These normalized ARF shift and normalized principal strain data demonstrated a strong correlation (Fig. 4b), indicating that the DEC technique provides a consistent method for detecting implant loading. The slopes of the ARF-strain curves were also analyzed for each specimen individually. The data indicate that the slopes appeared to increase slightly with each progressive osteotomy treatment for most of the tested specimens (Fig. 5c). However, none of the differences in ARF-strain slopes were statistically significantly ($p \geq 0.06$), suggesting that the ARF shifts were representative of plate strain. The mean sensitivity of the ARF measurement with respect to plate strain for all combined treatment groups was $-1.2\,\text{kHz}/\mu\varepsilon$ ($\pm 0.7\,\text{kHz}/\mu\varepsilon$ standard deviation).

The finite element model of the plated metatarsal predicted plate strains within one standard deviation of the experimental results for all four conditions (Fig. 2b). As expected, the strain magnitude increased as the amount of bone in the fracture region decreased. The model predicted relative plate deflections of 0.01, 0.10, 0.23, and 0.50 mm for the intact, 1CO, 1.5CO, and 2CO conditions, respectively.

The parametric study of the callus elastic modulus predicted that as the elastic modulus increased, the strain on the surface of the plate decreased, approximately following an exponential decay relationship (Fig. 6a). The plate strain: (1) was relatively unchanged and at a maximum for callus elastic moduli less than approximately 1 MPa, (2) decreased most dramatically when the callus elastic modulus ranged from 1 to 100 MPa, and (3) was relatively close to zero for moduli greater than 100 MPa. Curves of the plate strain versus relative plate deflection were nearly identical between the callus parametric simulations and the osteotomy simulations (replicating the experimental conditions; Fig. 6b).

DISCUSSION

Ultimately, the DEC method's utility in orthopaedic trauma applications is dependent upon its ability to detect changes in construct mechanical stability as a fracture heals over time, especially early in the healing process. The results of the experimental fracture healing model showed that the DEC method successfully measured an increase in the signal (ARF/load slope) with each progressively destabilized condition with good statistical fidelity, matching the results from the wired strain gage experimental preparations. The low coefficient of variance between test repetitions also indicated good repeatability of the measurement. The current study investigated the DEC method on plate and screw fixation of long bone fractures with compressive loading applied, which produced large changes in plate bending as the bone became destabilized due to changes in the neutral bending axis of the plate-bone construct relative to the axis of loading. The DEC technique is theoretically applicable for any fracture healing condition in which a load can be applied to produce a hardware deflection, such as a bending load applied to an intramedullary rod fixation.

It has previously been demonstrated that mechanical changes during fracture healing can be monitored by strain sensors on the surface of an orthopaedic plate.[9,21] Wired strain gage data using the current fracture healing model demonstrated differences between the various stages of fracture healing with high statistical fidelity. This confirmed that the experimental model appropriately simulated the expected changes in temporal fracture stiffness. The finite element simulations showed close agreement in the relationship between plate strain and plate deflection under a 500 N load between the replicated experimental model (with progressively larger osteotomies) and

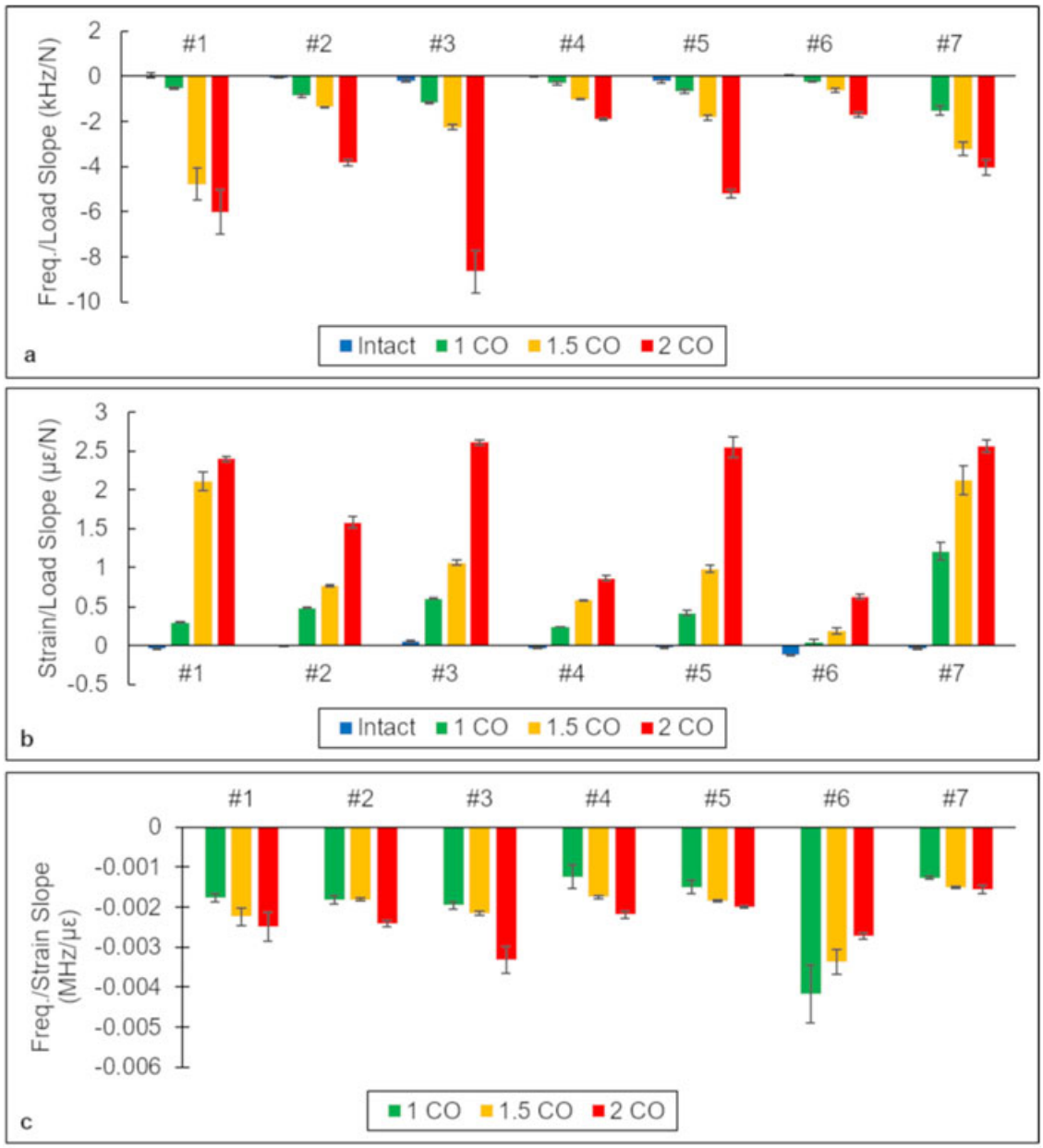

Figure 5. (a) Mean (with one standard deviation error bars) linear regression slope data of the ARF versus load curves for each tested specimen (#1-#7). The magnitude of the slope increased for each progressively destabilized treatment. (b) Linear regression slope data (mean and standard deviation) of the strain versus load curves, also showing an increase in slope for each progressively destabilized treatment. (c) Linear regression slope data (mean and standard deviation) of the ARF versus strain curves.

the callus stiffening model (Fig. 6b). These data provided further evidence that the experimental method of creating progressively larger osteotomies was a mechanically valid technique for simulating the in vivo healing process in which the apparent elastic modulus of the callus increases over time. The plate strain versus callus elastic modulus curve was fitted with a cubic spline, and the spline was used to predict the apparent callus elastic modulus corresponding to the average measured strain from the experimental tests. The 2CO, 1.5CO, 1CO, and intact conditions approximated average elastic moduli of 1.8, 13, 51, and >1 GPa, respectively, which falls within the range of callus tissue properties reported from nanoindentation tests (6 MPa to 1 GPa).[32] Furthermore, the 2CO, 1.5CO, and 1CO tests approximated the mechanical environment of relatively soft callus tissues, indicating that the experimental fracture healing test provided a good surrogate for studying healing during the early time period, when predicting the course of fracture healing is most critical.

It was expected that the ARF shift would provide an approximate measure for plate strain, and the plot of normalized ARF versus normalized strain indeed

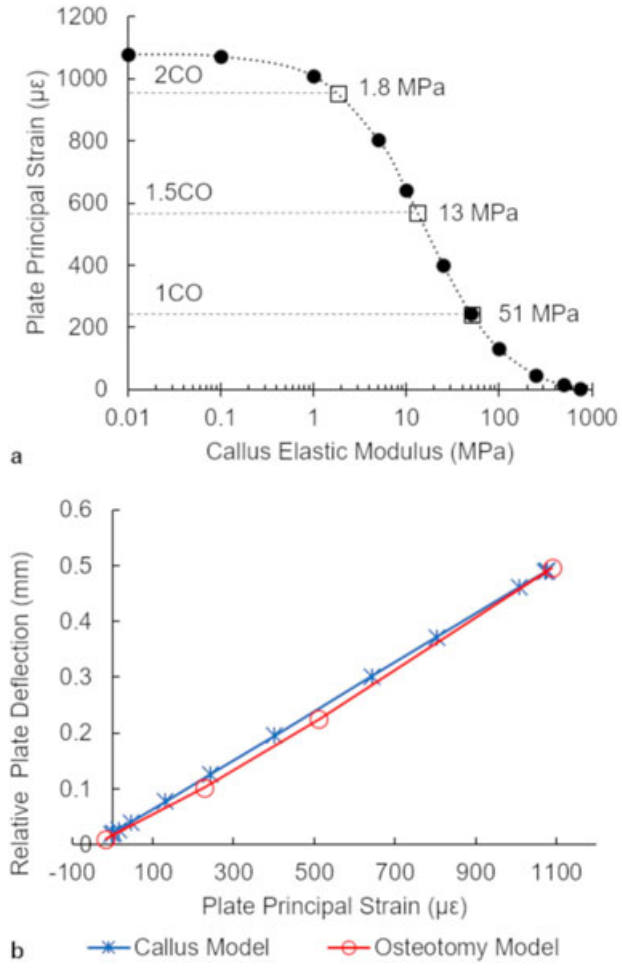

Figure 6. (a) Finite element predictions of plate principal strain for the parametric callus elastic modulus simulations. The elastic moduli corresponding to the mean experimental strains are indicated for the 1CO, 1.5CO, and 2CO conditions. (b) Finite element predictions of relative plate deflection versus plate strain, comparing the parametric callus model predictions with the osteotomy model predictions.

showed a strong, approximately linear correlation (Fig 4b). However, the mean sensitivity of the measurement (frequency/strain slope) appeared to increase from the 1CO to the 2CO conditions. Although not statistically significant, this increase in sensitivity can be supported theoretically by the nonlinear relationship between ARF and plate displacement,[23] even though it is approximately linear for all of the small displacement ranges measured. Additionally, the finite element simulations appeared to predict a slightly nonlinear relationship between plate strain and plate deflection for the replicated experimental model (Fig. 6b). This is likely due to the changing cross-sectional area of the model (and experimental specimens) with each osteotomy variant, producing an ipsilateral (with respect to the plate) shift in the location of the neutral axis of the bone/plate construct. This altered mechanical environment slightly affected the nearly linear relationship between plate strain and plate deflection. One specimen (#6) showed the opposite trend, with the mean frequency/strain slope decreasing from 1CO to 2CO, but that specimen also demonstrated the lowest magnitude strain and ARF shift, which was likely related to its alignment in the testing frame. The alignment affects the location of the applied load, and, subsequently, the bending moment on the plate and the plate's resultant strain and deflection under loading. Ultimately, the ARF data correlated well with strain, and the slightly higher sensitivity for the 2CO condition may indicate that the DEC measurement would be most sensitive during the early time period of healing, when the measurement would be most beneficial in the clinical setting.

There were some limitations to the experimental tests and computational analyses in the current study. The experimental fracture healing model used cadaveric isolated bone, which allowed for good control of the imposed mechanical loads, and it was a necessary initial study prior to a live animal testing. However, this in vitro setup may not simulate a clinical condition as well as a live animal model. The finite element model used for the callus stiffening analysis simplified the callus cross-sectional geometry by using an exact extrusion process to match that of the adjacent bone rather than the commonly observed in vivo callus geometry which typically protrudes beyond the periosteal borders of the native bone tissue. If a protruding callus had been represented with a larger cross-sectional area, it is expected that the predicted curve of plate strain decay with increasing elastic modulus (Fig. 6a) would have been shifted to the left (i.e., strain decaying at a lower elastic modulus). Nonetheless, the trends predicted by the model would have been similar, and the overall conclusions obtained using the current callus geometry would not have be affected.

The DEC method shows strong potential to supplement radiographic diagnostic monitoring of fracture healing because it provides a quantifiable measurement of the mechanical stability of the fracture. The measurement system is completely external to the body and is therefore advantageous when compared to implantable sensors, which carry long-term biocompatibility concerns. In contrast, DEC can potentially be used with any implantable fracture fixation hardware already in clinical use. The experiments and modeling efforts of the current study demonstrate that DEC can detect changes in mechanical stability that relate to the progression of healing in a fractured bone, which could inform on diagnostic predictions of delayed union or non-union. It is expected that further development of the DEC method may lead to widespread clinical translation of this technique.

AUTHORS' CONTRIBUTIONS

Kevin M. Labus contributed to the study design, experimental data acquisition and analysis, and drafting of the manuscript. Conor Sutherland contributed to computational data acquisition and analysis, and

drafting of the manuscript. Branislav M. Notaros and Milan M. Ilic contributed to study design, interpretation of data, and drafting of the manuscript. George Chaus and David Keiser contributed to the study design, interpretation of data, and critical revision of the manuscript. Christian M. Puttlitz contributed to the study design, interpretation of data, and drafting of the manuscript. All authors have read and approved the final submitted manuscript.

REFERENCES

1. Praemer A, Furner S, Rice D. 1999. Musculoskeletal conditions in the United States. Park Ridge, IL: American Academy of Orthopaedic Surgeons.
2. Dickson K, Katzman S, Delgado E, et al. 1994. Delayed unions and nonunions of open tibial fractures. Correlation with arteriography results. Clin Orthop Relat Res 302:189–193.
3. Dahabreh Z, Dimitriou R, Giannoudis PV. 2007. Health economics: a cost analysis of treatment of persistent fracture non-unions using bone morphogenetic protein-7. Injury 38:371–377.
4. Schmickal T, Von Recum J, Wentzensen A. 2005. Stiffness measurement of the neocallus with the Fraktometer FM 100. Arch Orthop Trauma Surg 125:653–659.
5. Webb J, Herling G, Gardner T, et al. 1996. Manual assessment of fracture stiffness. Injury 27:319–320.
6. Schmidhammer R, Zandieh S, Mittermayr R, et al. 2006. Assessment of bone union/nonunion in an experimental model using microcomputed technology. J Trauma 61: 199–205.
7. Miclau T, Lu C, Thompson Z, et al. 2007. Effects of delayed stabilization on fracture healing. J Orthop Res 25:1552–1558.
8. Thompson Z, Miclau T, Hu D, et al. 2002. A model for intramembranous ossification during fracture healing. J Orthop Res 20:1091–1098.
9. Stoffel K, Klaue K, Perren SM. 2000. Functional load of plates in fracture fixation in vivo and its correlate in bone healing. Injury 31:B37–B50.
10. Bergmann G, Deuretzbacher G, Heller M, et al. 2001. Hip contact forces and gait patterns from routine activities. J Biomech 34:859–871.
11. Bergmann G, Graichen F, Rohlmann A, et al. 1997. Hip joint forces during load carrying. Clin Orthop Relat Res 335: 190–201.
12. Graichen F, Bergmann G, Rohlmann A. 1999. Hip endoprosthesis for in vivo measurement of joint force and temperature. J Biomech 32:1113–1117.
13. Rohlmann A, Gabel U, Graichen F, et al. 2007. An instrumented implant for vertebral body replacement that measures loads in the anterior spinal column. Med Eng Phys 29:580–585.
14. Rohlmann A, Graichen F, Kayser R, et al. 2008. Loads on a telemeterized vertebral body replacement measured in two patients. Spine 33:1170–1179.
15. Rohlmann A, Graichen F, Weber U, et al. 2000. 2000 Volvo Award winner in biomechanical studies: monitoring in vivo implant loads with a telemeterized internal spinal fixation device. Spine 25:2981–2986.
16. Bergmann G, Graichen F, Bender A, et al. 2007. In vivo glenohumeral contact forces-measurements in the first patient 7 months postoperatively. J Biomech 40:2139–2149.
17. Bergmann G, Graichen F, Rohlmann A, et al. 2008. Design and calibration of load sensing orthopaedic implants. J Biomech Eng 130:021009.
18. Shah AD, Taylor SJ, Hua J. 2006. Correlation of radiographic and telemetric data from massive implant fixations. J Biomech 39:1304–1314.
19. Melik R, Perkgoz NK, Unal E, et al. 2008. Bio-implantable passive on-chip RF-MEMS strain sensing resonators for orthopaedic applications. J Micromech Microeng 18:115017.
20. Melik R, Unal E, Perkgoz NK, et al. 2010. Nested metamaterials for wireless strain sensing. IEEE J Sel Top Quantum Electron 16:450–458.
21. Mcgilvray KC, Unal E, Troyer KL, et al. 2015. Implantable microelectromechanical sensors for diagnostic monitoring and post-surgical prediction of bone fracture healing. J Orthop Res 33:1439–1446.
22. Symeonidis S, Whittow WG, Zecca M, et al. 2018. Bone fracture monitoring using implanted antennas in the radius, tibia and phalange heterogeneous bone phantoms. Biomed Phys Eng Expr 4:045006.
23. Labus KM, Notaros BM, Ilic MM, et al. 2018. A coaxial dipole antenna for passively sensing object displacment and deflection for orthopaedic applications. IEEE Access 6:68184–68194.
24. Gadomski BC, Lerner ZF, Browning RC, et al. 2016. Computational characterization of fracture healing under reduced gravity loading conditions. J Orthop Res 34: 1206–1215.
25. Gadomski BC, Mcgilvray KC, Easley JT, et al. 2018. An investigation of shock wave therapy and low-intensity pulsed ultrasound on fracture healing under reduced loading conditions in an ovine model. J Orthop Res 36:921–929.
26. Gadomski BC, Mcgilvray KC, Easley JT, et al. 2014. Partial gravity unloading inhibits bone healing responses in a large animal model. J Biomech 47:2836–2842.
27. Lang SB. 1970. Ultrasonic method for measuring elastic coefficients of bone and results on fresh and dried bovine bones. IEEE T Bio-Med Eng Bm 17:101.
28. Lipson SF, Katz JL. 1984. The relationship between elastic properties and microstructure of bovine cortical bone. J Biomech 17:231.
29. Mittra E, Rubin C, Qin YX. 2005. Interrelationship of trabecular mechanical and microstructural properties in sheep trabecular bone. J Biomech 38:1229–1237.
30. Nafei A, Danielsen CC, Linde F, et al. 2000. Properties of growing trabecular ovine bone – Part I: mechanical and physical properties. J Bone Joint Surg Br 82b:910–920.
31. Nafei A, Kabel J, Odgaard A, et al. 2000. Properties of growing trabecular ovine bone – Part II: architectural and mechanical properties. J Bone Joint Surg Br 82b:921–927.
32. Leong PL, Morgan EF. 2008. Measurement of fracture callus material properties via nanoindentation. Acta Biomater 4:1569–1575.